*SF2A 2016*
*C. Reylé, J. Richard, L. Cambrésy, M. Deleuil, E. Pécontal, L. Tresse and I. Vauglin (eds)*

# THE GASEOUS PROTO-CLUSTER AS A PRODUCT OF GRAVO-TURBULENT INTERACTION: MODIFIED LOCAL ENVIRONMENT FOR STELLAR CLUSTER FORMATION?

Y.-N. Lee[1] and P. Hennebelle[1,2]

**Abstract.** Stars are often observed to form in clusters, while the formation of the gaseous proto-cluster precedes that of the stellar cluster. We discuss the assembly of gas via gravo-turbulent reprocessing inside collapsing molecular clouds, and demonstrate that virial equilibrium is established for the gaseous proto-cluster, of which the higher density is favorable for clustered star formation, and that some physical characteristics of the stellar cluster are inherited from the gaseous proto-cluster. We introduce an analytical two-dimensional virial model to account for the quasi-stationary accreting gaseous proto-cluster which has non-negligible rotation. Results are compared to observations and simulations and the fact that gaseous proto-clusters lie on an equilibrium sequence may imply that star formation could be to some extent disentangled from larger scale physics, offering an encouraging explanation for the universality of IMF.

Keywords: proto-cluster, star formation, cluster, gravity, IMF

## 1 Introduction

Star formation is a hierarchical process with involves a density change over orders of magnitude. Galaxy dynamics at kilo-parsec scales causes density concentrations through shocks and shearing forces. The structure forms from giant molecular associations or HI super-clouds down to parsec-scale molecular clouds (McKee & Ostriker 2007). Inside molecular clouds, further density concentration creates site of clustered star formation. These mass concentrations are often referred to as star-forming clumps, in which high star formation activity is observed while the stars are stilled embedded inside the gas. At a later stage of the stellar activities, massive stars start to combust violently or even reach the end of the lives, and therefore blowing the gas away by injecting energy into the interstellar medium (ISM). The formation phase of a cluster is thus terminated by expulsion of all the gas available for forming stars. It has been suggested in previous studies that most stars are formed in clusters (Lada & Lada 2003; Allen et al. 2007; McKee & Ostriker 2007). Depending on the amount of energy, the end product of this process is either an open cluster, which is gas free, with the stars directly observable, or individual stars dissociated from the cluster, becoming field stars. This mode of clustered star formation is, therefore, important for understanding the origin of stellar statistical properties, such as the initial mass function (IMF), which has a fundamental impact on the amount of feedback energy available from massive stars and also the number solar-type stars that can harbor life.

Given the large variation in density, which translates into free-fall time, and the spatial scales concerned. In order to properly address the physical processes that are important at different scales, star formation is often studied step by step. This study is focused on the gas assembly phase of cluster formation, where the interaction between gravity and turbulence are most dominating physical processes. The tight correlation between the mass-size relation of star-forming clumps and that of the stellar clusters (Pfalzner et al. 2016) also suggest that star formation should be studied in conditions that correspond to these dense entities*. Fall et al. (2010) inferred from observational results of molecular lines and dust continuum a stellar cluster mass-size relation $R \propto M^{0.38}$

[1] Laboratoire AIM, Paris-Saclay, CEA/IRFU/SAp – CNRS – Université Paris Diderot, 91191 Gif-sur-Yvette Cedex, France
[2] LERMA (UMR CNRS 8112), Ecole Normale Supérieure, 75231 Paris Cedex, France

*Both the terms star-forming clump and gaseous proto-clusters refer to dense substructures inside molecular clouds, where most star formation takes place, and are used indifferently inside this text.

for mass range from $10^2$ to $10^4$ solar masses. Similar studies from the ARLASGAL survey (Urquhart et al. 2014) concluded $R \propto M^{0.50}$. Given the data dispersion, this power-law exponent is compatible with value between 0.4 and 0.6. Previous studies (Hennebelle 2012; Matzner & Jumper 2015) tried to analytically describe the quasi-static growth of proto-cluster by balancing gravitational and turbulent forces, and studies the the proto-stellar population resulting from such environment. Meanwhile, Pfalzner (2011) regarded this mass-size relation as a growth sequence. So far these models have ignored rotation, which, however, has been observed in several stellar clusters (Hénault-Brunet et al. 2012; Davies et al. 2011; Mackey et al. 2013). Indeed structures forming from collapse usually show important rotation due to angular momentum conservation. We therefore follow a similar idea to Hennebelle (2012), while taking the rotation and turbulence into account to develop an analytical model to infer gaseous proto-cluster properties from those of the parent molecular cloud. Given the small infall and the observed sequence (Fall et al. 2010; Urquhart et al. 2014), an equilibrium, at globally equilibrium assumption is highly plausible. Our model applies to low-mass clusters, and those with mass above $10^4$ are beyond the scope of our discussion since more massive clumps tend to evolve more quickly and form massive stars that, in turn, disrupt the cloud via feedback. We caution that although we refer to this gaseous proto-cluster as the first phase of stellar cluster formation, this is actually a continuous process: the stars start to form as the gas proto-cluster is still accreting and finally take over after the gas expulsion. In this picture, the gaseous proto-cluster is globally in equilibrium, while density fluctuations therein cause local infall to form stars. This study is restricted to the earliest stage where the effects of the stars are less important.

## 2 Two-dimensional model: Modified virial theorem

We present a simple analytical model to describe the gaseous proto-cluster formation from a collapsing molecular cloud: a virial model, adapted to the turbulent and rotational kinematics of the cluster under mass accretion. We propose that a gaseous proto-cluster is in global virial equilibrium, and the rotational and turbulent kinetic energy support against self-gravity and ram pressure confinement. The rotation results from angular momentum conservation under collapse, while the turbulence is sustained by the accreting gas and dissipates through turbulent cascade. We start by deducing the two-dimensional virial theorem for an ellipsoidal structure with rotation and turbulence, and then discuss the energy balance from accretion and turbulent dissipation. The mass accretion rate and the specific angular momentum are evaluated as properties of the parent cloud. Finally, we present the mass-size relation predicted by the model.

### *2.1 Two-dimensional virial theorem of the gaseous proto-cluster*

Rotation introduces non-isotropic motions which makes that the geometry is no longer spherical. We consider an oblate ellipsoid that has its minor-axis coinciding with the rotational axis. The three semi-axes are $R = R > H$. Neglecting the thermal and magnetic terms terms for simplicity, we calculate the virial integral of the system in two dimensions, by taking the inner product of the momentum equation $\rho d_t \vec{v} = -\rho \nabla \phi$ with the $\vec{r}$ and $\vec{z}$ vectors in the cylindrical coordinate before integrating over the volume of the ellipsoid. The integration of the inner product with $\vec{r}$ gives:

$$\frac{1}{2}\partial_t^2 \int_V \rho r^2 dV + \frac{1}{2}\partial_t \int_S \rho\, r^2 \vec{v}\cdot d\vec{S} + \int_S v_r r \rho \vec{v}\cdot d\vec{S} - \int_V \rho v_{2\mathrm{d}}^2 dV = -\frac{3}{5}\frac{GM^2}{R}\left[\frac{\cos^{-1}(\eta)}{(1-\eta^2)^{\frac{3}{2}}} - \frac{\eta}{1-\eta^2}\right] = -\frac{GM^2}{R}u_r(\eta), \tag{2.1}$$

where $v_{2\mathrm{d}}$ is the velocity dispersion in the $x-y$ plane, and $v_r$ is the velocity dispersion in the $\vec{r}$ direction; $\eta = \frac{H}{R}$ represents the aspect ratio of the ellipsoid. In the $\vec{z}$ direction we obtain

$$\frac{1}{2}\partial_t^2 \int_V \rho z^2 dV + \frac{1}{2}\partial_t \int_S \rho\, z^2 \vec{v}\cdot d\vec{S} + \int_S v_z z \rho \vec{v}\cdot d\vec{S} - \int_V \rho v_{1\mathrm{d}}^2 dV = -\frac{3}{5}\frac{GM^2}{R}\left[\frac{\eta}{1-\eta^2} - \frac{\eta^2\cos^{-1}(\eta)}{(1-\eta^2)^{\frac{3}{2}}}\right] = -\frac{GM^2}{R}u_z(\eta), \tag{2.2}$$

where $v_{1d} = v_z$ is the velocity dispersion in the $\vec{z}$ direction.

Virial equilibrium is reached when the time derivative terms are zero. The third term on the left-hand side of both equations is the counterpart of the ram pressure term in the spherical model (Hennebelle 2012), while the geometry renders its interpretation less obvious since we are ignorant of the mass infall pattern. But its

impact is effectively less import and is neglected in this discussion. Therefore we have the equations for virial equilibrium in two dimensions by simplifying Eqs. (2.1) and (2.2) as

$$Mv_{\rm 2d}^2 = \frac{GM^2}{R}u_r(\eta) \quad \text{and} \quad Mv_{\rm 1d}^2 = \frac{GM^2}{R}u_z(\eta). \tag{2.3}$$

### 2.2 The energy equilibrium of an ellipsoidal cluster

In an accreting system, the turbulence is driven by the gravitational energy released from the accreted material (Klessen & Hennebelle 2010; Goldbaum et al. 2011), and it dissipates through the turbulent cascade on the timescale of the crossing time of the system. The turbulent energy is found by balancing the driving and the dissipation. Considering our ellipsoid with uniform density, the gravitational potential energy is given by the Legendre elliptical integral of the first kind $F(\varphi|k) = \int_0^\varphi \frac{d\theta}{\sqrt{1-k^2\sin\theta^2}}$:

$$E_{\rm grav} = \frac{3}{10}GM^2\frac{2}{\sqrt{R^2-H^2}}\cos^{-1}\left(\frac{H}{R}\right) = \frac{3}{5}\frac{GM^2}{R}\frac{\cos^{-1}(\eta)}{\sqrt{1-\eta^2}} = \frac{GM^2}{R}u_g(\eta).$$

The rate of gravitational that transforms into turbulent energy is

$$\dot{E}_{\rm grav} = \epsilon\frac{GM^2}{R}u_g(\eta)\left(\frac{2\dot{M}}{M} - \frac{\dot{R}}{R} + \frac{u_g'(\eta)\dot{\eta}}{u_g(\eta)}\right), \tag{2.4}$$

where the unknown factor $\epsilon \leq 1$ stands for the turbulence-driving efficiency, while part of the energy is dissipated at the accretion shock. Absorbing the second and third terms in the parenthesis into the uncertainties of accretion driving efficiency, we obtain a simplified expression

$$\dot{E}_{\rm grav} = \epsilon_{\rm acc}\frac{2GM\dot{M}}{R}u_g(\eta). \tag{2.5}$$

The turbulence dissipates via turbulent cascade on the crossing time of the system $\tau_{\rm diss}$, while the directional energy distribution and the relevant scale is less well understood in ellipsoidal geometry. We discuss two assumptions, which introduces two sets of equations with similar form but different coefficients. Firstly, we assume that the turbulence is anisotropic and that the turbulent energy follows the inertial regime of the Kolmogorov spectrum even though the structure is not spherically symmetric, that is, the energy cascades down length scales at the same rate and is eventually dissipated.

$$\dot{E}_{\rm diss} = \frac{3}{2}M\sigma_H^2/\tau_{\rm diss} = \frac{3}{2}M\sigma_H^2/\frac{2H}{\sigma_H} = \frac{3}{4}M\sigma_R^3/R. \tag{2.6}$$

Secondly, we make an alternative assumption that the inertial range at which the energy is dominating is reached at scales smaller than the cluster size, the turbulence should be isotropic. By assuming the dominating scale $\epsilon_{\rm diss}H < H$, we obtain

$$\dot{E}_{\rm diss} = \frac{3}{2}M\sigma_R^2/\tau_{\rm diss} = \frac{3}{2}M\sigma_R^2/\frac{2\epsilon_{\rm diss}H}{\sigma_R} = \frac{3}{4}M\sigma_R^3/\epsilon_{\rm diss}\eta R. \tag{2.7}$$

The rotation provides support only in the directions perpendicular to the rotational axis. Using the averaged specific angular momentum $j$, the rotational energy of the cluster is $2E_{\rm rot} = \frac{5}{2}M\left(\frac{j}{R}\right)^2$. The factor $\frac{5}{2}$ comes from uniform density and rigid body assumptions, which we verified with simulations to be not far from being realistic. Using Eqs. (2.3, 2.5, 2.6), and (2.7) while splitting the two-dimensional motion perpendicular to the short axis into rotation and turbulence, we obtain the equation set to be solved, i.e.,

$$\frac{5}{2}\left(\frac{j}{R}\right)^2 + s_r(\eta)\sigma^2 = \frac{GM}{R}u_r(\eta) \tag{2.8a}$$

$$s_z(\eta)\sigma^2 = \frac{GM}{R}u_z(\eta) \tag{2.8b}$$

$$\dot{E}_{\rm diss}/M = d(\eta)\frac{\sigma^3}{4R} = \dot{E}_{\rm grav}/M = \epsilon_{\rm acc}\frac{2G\dot{M}}{R}u_g(\eta), \tag{2.8c}$$

where the geometrical factors $s_r$, $s_z$, and $d$ are described in Eqs. (2.6) and (2.7) for two cases. The factors $u_r$, $u_z$, and $u_g$ are functions of $\eta$ of the ellipsoid, as shown in Fig. 1. The essential idea is to decompose the gravitational potential resulting from force in different directions. It could be readily verified that $u_r(\eta) + u_z(\eta) = u_g(\eta)$ and that $u_g(1) = \frac{3}{5}$, which corresponds to the spherical case.

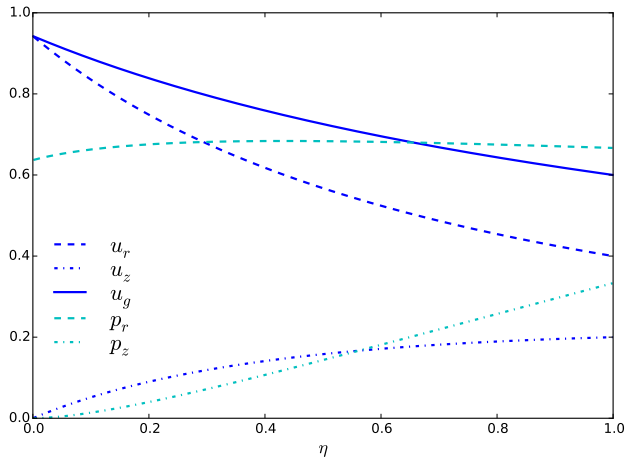


Fig. 1: Gravitational potential in blue curves (solid: complete potential $u_g$, dashed: $u_r$, dot-dashed: $u_z$) and the ram pressure factors in cyan as functions of the ellipsoid aspect ratio $\eta$.

### *2.3 Accretion rate and angular momentum*

In order to solve the equilibrium equations, we estimate the mass accretion rate and angular momentum as functions of the cluster mass, or more precisely, the cloud mass.

The mass accretion rate can be estimated through simple free fall arguments, while assuming that in a cloud experiencing inside-out collapse, the mass-flux rate is almost constant at any radius and comparable to the cloud surface. This could be verified with some analytical calculations as well as from simulations. The left panel of Fig. 2 shows the gaseous proto-cluster mass accretion rate plotted against mass in a molecular cloud of $10^4$ solar mass collapsing onto several final radii $r_f$, corresponding to the range of the proto-cluster radius in our simulations. After the gaseous proto-cluster mass reaches over $10^3$ $M_\odot$, the accretion rate becomes weakly dependent on the cluster mass for any cluster radius and approaches a value that is characteristic of the cloud mass. It is therefore reasonable to estimate the cluster accretion rate with the cloud mass and from we obtain

$$\dot{M}_0 \propto M_{\rm c}\sqrt{\rho_{\rm c}}, \tag{2.9}$$

where $M_{\rm c}$ and $\rho_{\rm c}$ are the cloud mass and density. Consider a molecular cloud following the Larson relations (Larson 1981; Falgarone et al. 2004, 2009; Hennebelle & Falgarone 2012; Lombardi et al. 2010)

$$\rho_{\rm c} \propto R_{\rm c}^{-\gamma} \quad \text{and} \quad \sigma_{\rm c} \propto \sqrt{\frac{M}{R}} \propto R_{\rm c}^{1-\frac{\gamma}{2}}, \tag{2.10}$$

where different values of $\gamma$ (typically around 0.7 or 1) are quoted in the literature. We obtain

$$\dot{M}_0 \propto M_{\rm c}\sqrt{\rho_{\rm c}} \propto R_{\rm c}^3\ \rho_{\rm c}^{1.5} \sim R_{\rm c}^{3-1.5\gamma} \propto M_c^{(6-3\gamma)/(6-2\gamma)}. \tag{2.11}$$

With $\gamma = 1$ or 0.7, we get $\dot{M}_0 \propto M_c^{\gamma_{\dot{M}}}$, where $\gamma_{\dot{M}} = 0.75$ or 0.85, respectively. We multiply this accretion rate by an empirical correction in the presence of turbulence, which behaves like a dilution factor $(1-\kappa)$, where $\kappa = E_{\rm turb}/E_{\rm grav}$ is the ratio between turbulent kinetic energy and gravitational energy of the cloud. A numerical evaluation is made for the cloud of $10^4$ solar mass, obtaining

$$\dot{M} = \dot{M}_0\sqrt{1-\kappa} = 4.0\times10^{-3}\ {\rm M}_\odot\ {\rm yr}^{-1}\left(\frac{\alpha_{*,c}M_*}{10^4{\rm M}_\odot}\right)^{\gamma_{\dot{M}}}\sqrt{1-0.35\left(\frac{\sigma_{\rm rms}}{\sigma_{\rm vir}}\right)^2}, \tag{2.12}$$

where $\alpha_{*,\rm c} = M_{\rm c}/M_*$ is the cloud-cluster mass ratio. An example of mass accretion rate evaluated at radius 1 pc, corresponding to $r_f/r_0 = 0.13$, is shown in the right panel of Fig. 2 for four simulations with different levels of turbulent support. This empirical correction for turbulent support is very simplistic but gives an error within a factor 2, and the four turbulence levels cover a large range of accretion rates, which all give reasonable mass-size relations. Thus this accretion rate approximation does not affect the results too much.

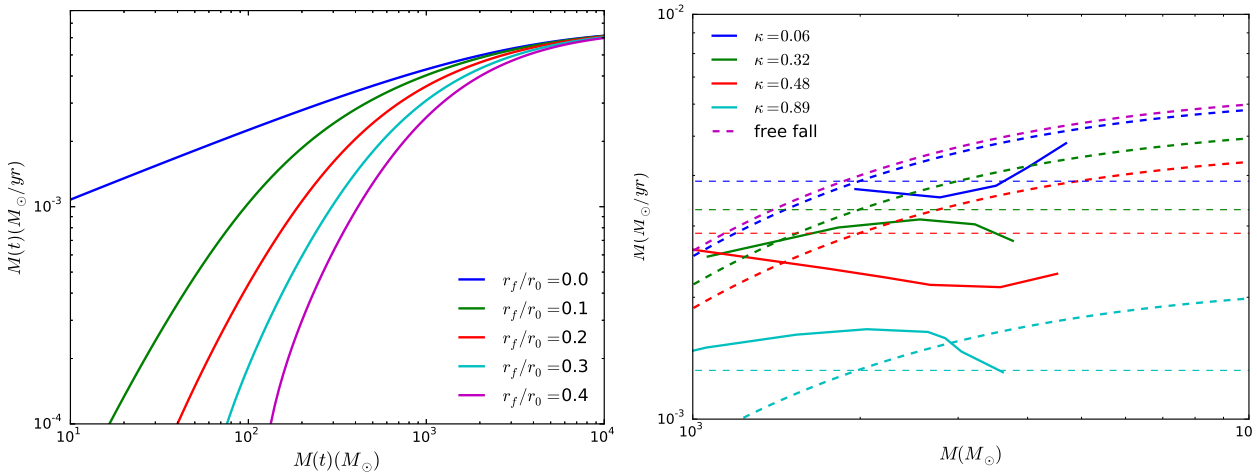


Fig. 2: **Left:** Mass accretion rate plotted against mass for several final radius values $r_f/r_0$ inside a $10^4$ $M_\odot$ cloud, assuming the interior of the cloud collapses in free fall. The radius at which $\dot{M}$ is evaluated increases from the top to the bottom curve. **Right:** Mass accretion rate plotted against mass at $r = 1$ pc. The solid curves represent values evaluated in simulations with different levels of turbulent support. The dashed curve in magenta is the analytical solution for a $10^4$ $M_\odot$ cloud in free fall. The empirically corrected accretion rate $\sqrt{1-\kappa}$ is plotted in dashed curves. The accretion rate is approximated to be constant at its value at $M_* = 2 \times 10^3$ $M_\odot$.

The estimation of angular momentum follows the cancelation between turbulent vortices, which usually results in some residual rotation, that is then amplified by the collapse of the molecular cloud. We take a characteristic rotational velocity proportional to the turbulent velocity dispersion and follows the scaling law $v_{\rm rot} \propto v_{\rm rms}(r/r_0)^{0.5}$ (Dib et al. 2010; Burkert & Bodenheimer 2000). Using the Bonnor-Ebert-like density profile in our simulations (Lee & Hennebelle 2016a)

$$\rho(r) = \frac{\rho_0}{1+\xi^2},\ \xi = \frac{r}{r_0} \in [0, \xi_{\rm ext}], \tag{2.13}$$

where $\xi_{\rm ext} = r_{\rm ext}/r_0 = 3$ and assuming random rotational axis in spherical shells, we have the averaged specific angular momentum inside a sphere of radius $r$ with the density profile described in Eq. (2.13),

$$\bar{j}(r) = \left[\frac{\int_{M(r)} (v_{rot} r)^2 dm}{\int_{M(r)} dm}\right]^{\frac{1}{2}} = 0.22\ v_{\rm rms}\ r_0\ \frac{1}{2}\left[\frac{\xi^4 - 2\xi^2 + 2\log(1+\xi^2)}{\xi - \arctan(\xi)}\right]^{\frac{1}{2}}. \tag{2.14}$$

The constant is calibrated with the simulations. The average specific angular momentum plotted against mass at varying radius is plotted in Fig. 3 for the initial condition of four runs (solid curves) with varying levels of turbulent support, as well as the analytical solutions (dashed curves) with corresponding $v_{\rm rms}$. The specific angular momentum roughly has the dependence $\bar{j}(r) \propto M(r)^{0.59}$ in the mass range of our interest ($10^3 - 10^4$ $M_\odot$). We do the consider the lost by angular momentum transport in our model since this effect is not very important at the cluster scale. The averaged specific angular momentum in the gaseous proto-cluster thus has the form:

$$j_* \propto j_{\rm c}\left(\frac{M_*}{M_{\rm c}}\right)^{0.59} \propto \sigma_{\rm c}\ R_{\rm c}\ \alpha_{*,{\rm c}}^{-0.59} \propto M_c^{(4-\gamma)/(6-2\gamma)}\ \alpha_{*,{\rm c}}^{-0.59}. \tag{2.15}$$

The last approximation comes from the Larson relations (Eqs. (2.10)). Applying physical values gives

$$j_* = 6.7 \times 10^{19} {\rm m^2 s^{-1}} \frac{\sigma_{\rm rms}}{\sigma_{\rm vir}} \left(\frac{\alpha_{*,c} M_*}{10^4 {\rm M_\odot}}\right)^{\gamma_j} \alpha_{*,{\rm c}}^{-0.59}, \tag{2.16}$$

where $\gamma_j = 0.75$ or $0.72$ corresponding to $\gamma = 1$ or $0.7$.

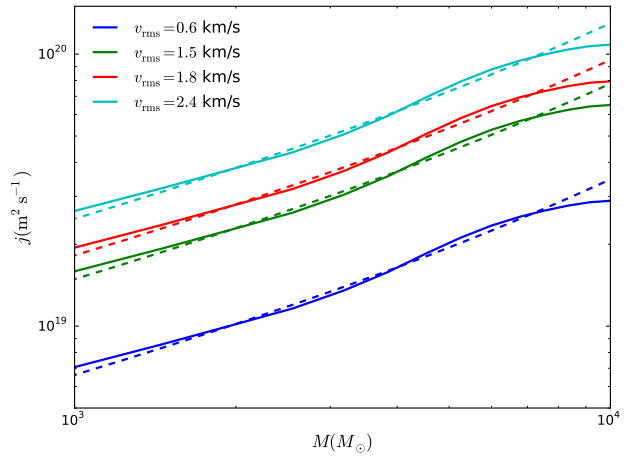


Fig. 3: Specific angular momentum plotted against mass contained inside varying radius. Solid curves represent the values calculated from the initial condition of the simulation. Dashed curves show the values estimated analytically. Values from four simulations with various initial turbulent supports are shown, and the specific angular momentum scales with the velocity dispersion.

### *2.4 Results and comparisons*

Given the parameters $\dot{M}$ and $j$, solving Eqs. (2.8) to infer the three variables $R$, $\eta$, $\sigma^2$ for a given mass in equilibrium is equivalent to solving for $\eta$ and $R$ from equations

$$f(\eta) = \frac{8\frac{5}{2}^{\frac{3}{2}} j^3 \dot{M}}{G^2 M^3} = \begin{cases} u_z^{\frac{3}{2}}(u_r - \frac{1+\eta^{\frac{2}{3}}}{\eta^{\frac{2}{3}}}u_z)^{\frac{3}{2}}(1+2\eta^{\frac{2}{3}})/(\epsilon_{\rm acc}\eta u_g) \\ u_z^{\frac{3}{2}}(u_r - 2u_z)^{\frac{3}{2}}3/(\epsilon_{\rm diss}\epsilon_{\rm acc}\eta u_g) \end{cases} \quad \text{and } R = \frac{5j^2}{2GM} r(\eta) = \begin{cases} \frac{5j^2}{2GM}\left(u_r - \frac{1+\eta^{\frac{2}{3}}}{\eta^{\frac{2}{3}}}u_z\right)^{-1} \\ \frac{5j^2}{2GM}(u_r - 2u_z)^{-1} \end{cases}, \tag{2.17}$$

where the upper row is the anisotropic solution and the bottom row the isotropic one. The functions $f(\eta)$ and $r(\eta)$ are geometrical factors that depend on $\eta$. The solution occurs at the intersection of $f(\eta)$ and a constant determined by $M$, $\dot{M}$, and $j$ as seen in Eqs. (2.17). Since $f(\eta)$ is first increasing and then decreasing in the interval $\eta \in [0,1]$, two solutions coexist when there are solutions. The solution with a higher value of $\eta$ is physical because it reduces to the spherical case when the angular momentum goes to zero. The recovered $\eta$ value in turn gives the radius of the gaseous proto-cluster.

The gaseous proto-cluster mass-size relation is governed by several parameters. We apply some canonical values to illustrate the solution properties in Fig 4. Three cloud-cluster mass ratios $\alpha_{*,\rm c} = 1, 2, 3$ are used for virialized molecular clouds, i.e., $\sigma_{\rm rms}/\sigma_{\rm vir} = 1$, in Eqs. (2.12 and 2.16). The canonical turbulence driving efficiency $\varepsilon = 0.5$ is used; see Eqs. (2.7, 2.8, and 2.17), $\varepsilon = \epsilon_{\rm acc}$ and $\varepsilon = \epsilon_{\rm diss}\epsilon_{\rm acc}$, respectively. The resulting mass-size relation is shown in Fig. 4 for two $\gamma$ values. The dispersion of observations is compatible with a large range of the model parameters, guaranteeing the robustness of our model prediction regardless of some poorly controlled factors. Our model yields a $R \propto M^{0.5}$ relation for $\gamma = 1$ and $R \propto M^{0.42-0.44}$ for $\gamma = 0.7$. These power-law exponents are compatible with those from Fall et al. (2010, 0.38) and Urquhart et al. (2014, 0.50). We overplot the model with their star-forming clumps. The trend is very closely reproduced. The mass-size relations that we obtained is thus robust despite our ignorance of the properties of the turbulence, which only introduces a slight change in aspect ratio of the proto-clusters. The curves do not represent evolutionary sequences. After a gaseous proto-cluster reaches equilibrium, it evolves toward sequences with smaller $\alpha_{*,\rm c}$ presuming that the parent cloud is not accreting mass much faster than the gaseous proto-cluster. We trace in yellow the gaseous proto-cluster formed inside a $10^4$ $\mathrm{M}_\odot$ cloud in Fig. 4, which is indicative as an evolutionary sequence following $R \propto M$. A clump does not migrate too much on this equilibrium sequence during their lifespan, and the mass-size relation observed for star-forming clumps is rather a result of gaseous proto-clusters forming from a range of different gas reservoir than an evolutionary track.

We evaluate the proto-cluster mass and size from simulations and over plot the results on the model predictions in Fig. 5. The level of turbulent support is represented by the virial parameter $\alpha_{\rm vir} = 2E_{\rm kin}/E_{\rm grav}$.

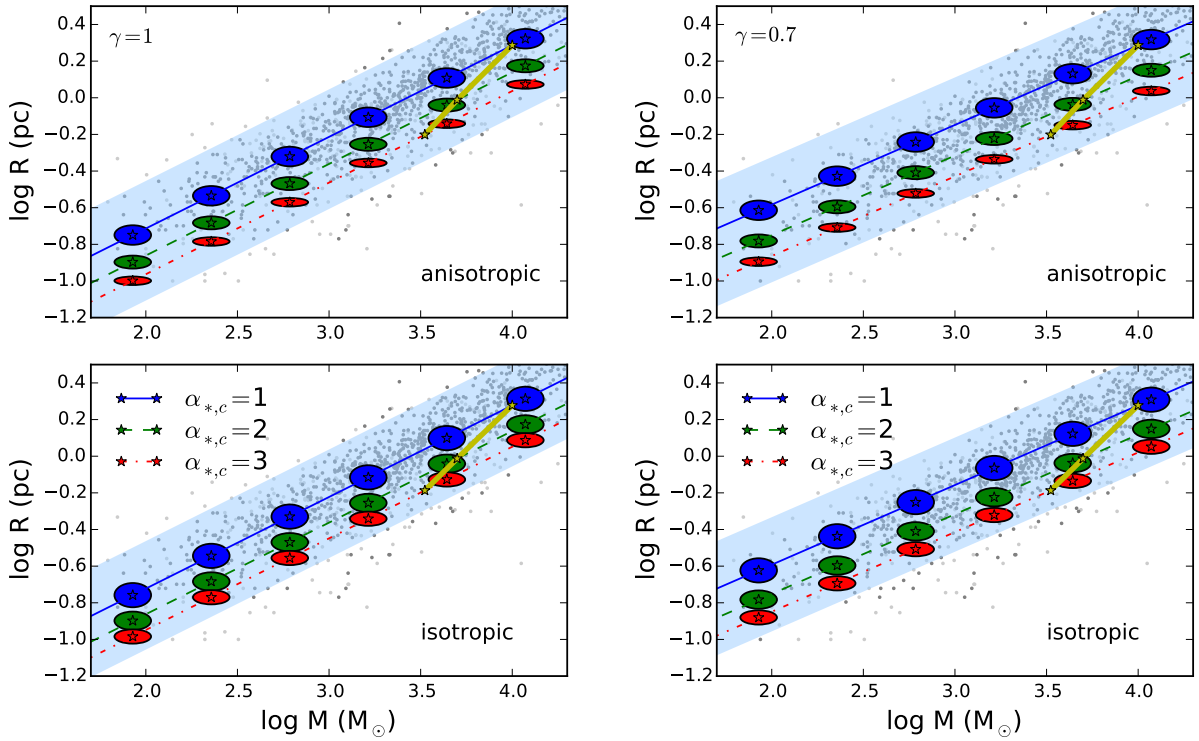


Fig. 4: **Left:** Mass-size relation of ellipsoidal clusters, shown with cloud-cluster mass ratio $\alpha_{*,c} = 1, 2, 3$, plotted with blue solid, green dashed, red dot-dashed lines, respectively, using anisotropic turbulence following Kolmogorov spectrum (upper panel) and isotropic turbulence (lower panel). The turbulence efficiency $\varepsilon = 0.5$ is used, and the shadowed region represents the range of solutions for $\varepsilon \in [0.2, 0.7]$. The radius of the cluster decreases with increasing $\varepsilon$. The elliptical patches represent the form of the clusters. With the molecular cloud density-size relation $\rho \propto R^{-1}$, the clusters follow a $R \propto M^{0.5}$ trend for a given $\alpha_{*,c}$. The gaseous proto-cluster corresponding to $10^4$ $M_\odot$ parent cloud is traced in yellow, indicating of an evolutionary sequence roughly following $R \propto M$. The radius of the gaseous proto-cluster does not depend too much on the underlying assumption of the turbulent energy distribution, while the aspect ratio is smaller in the anisotropic case since there is relatively less turbulent support in the vertical direction. The dots are the observed star-forming clumps from Fall et al. (2010) and Urquhart et al. (2014). **Right:** Same plots as figures on the left for gaseous proto-clusters inside parent clouds following $\rho \propto R^{-0.7}$ relation. The mass-size relation follows $R \propto M^{0.42-0.44}$.

The angular momentum and mass accretion rate are calculated accordingly for each case. We show models with values $\gamma = 1$ and 0.7. The results show that the proto-cluster could be identified at a relative early stage when the mass is still small, and that as it accretes mass, it arrives on the sequence where virial equilibrium is reached. The model is not in good coherence with simulation results at early time, possibly because the time-dependent terms and ram pressure are still relatively important and should not be neglected, while we use quasi-stationary assumptions. Once the mass is large enough, the simulations are in good agreement with the model. The case with $\alpha_{\rm vir} = 0.12$ is probably too strongly accreting owing to the weak kinetic support, thus this case does not correspond well to the quasi-stationary model.

### *2.5 The IMF peak position*

The theoretical prediction of the core mass function (CMF) peak position (Hennebelle & Chabrier 2013) depends on the Jeans mass and the Mach number of the star-forming gas. We calculate the Jeans mass $M_{\rm J} = \pi^{5/2} c_s^3 / 6\sqrt{G^3 \rho}$ (thin curves) and the predicted CMF peak mass $M_{\rm peak} = M_{\rm J}/(1 + b^2 \mathcal{M}^2)$ (thick curves), which are shown in Fig. 6, from the proto-cluster properties predicted by our model. A canonical value $b = 0.5$ is used (Federrath et al. 2010). We present the result with two $\gamma$ values (see Eq. (2.10)) and two polytropic equation of state $P \propto \rho^\Gamma$ with $\Gamma = 1$ or 0.85. With increasing mass, the Jeans mass increases with decreasing density. On the other hand, the turbulence increases with gaseous proto-cluster mass and gives a reasonable IMF peak prediction assuming that CMF and IMF peaks coincide. In the mass range between $10^2$ and $10^4$

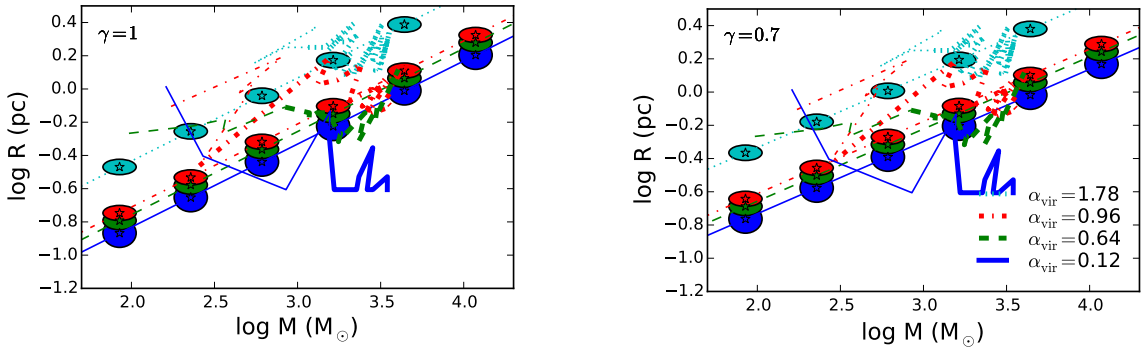


Fig. 5: **Left:** Mass-size relation of ellipsoidal clusters. The proto-cluster identified from simulations are over-plotted with models of the corresponding levels of turbulence with $\gamma = 1$ . Canonical values of cloud-cluster mass ratio $\alpha_{*,c} = 3$ and $\varepsilon = 0.5$ are used along with isotropic turbulence. The velocity dispersion increases from the bottom to the top curve. Simulation results at time before 2 Myr are plotted with thin lines. The model is in good agreement with simulation only after the proto-cluster gains enough mass, possibly implying that the time dependent terms and ram pressure should not be neglected at early stage. **Right:** Same as left panel but with $\gamma = 0.7$.

solar mass, where most clusters are observed, the predicted IMF peak value is around $0.1 - 0.3$ $M_\odot$ with less than 1 dex variation.

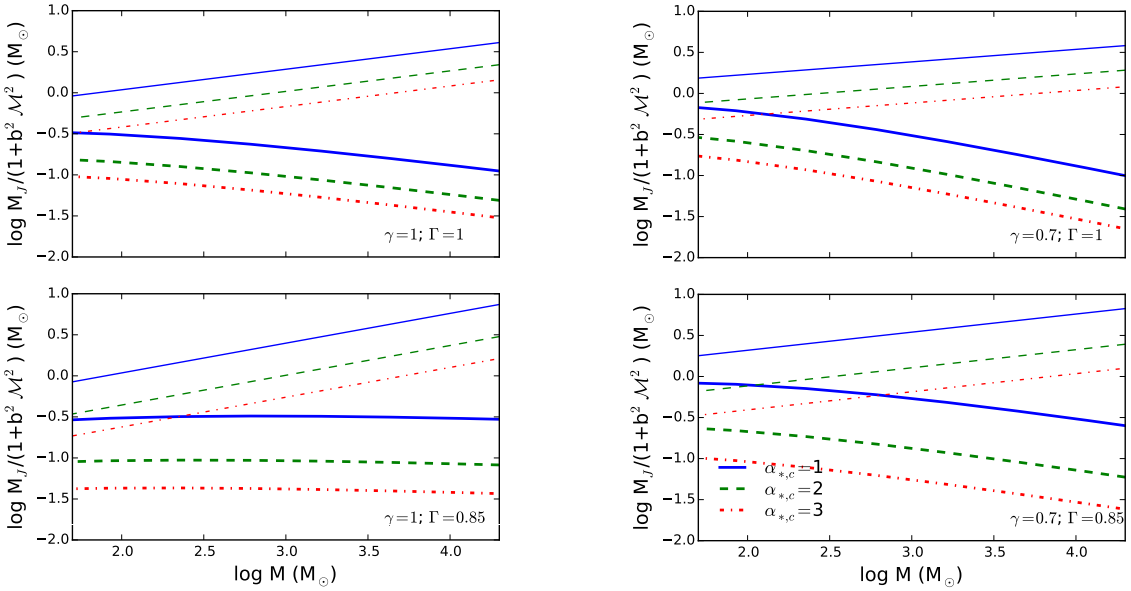


Fig. 6: Initial mass function peak prediction from proto-cluster model with isotropic turbulence for cloud-cluster mass ratio $\alpha_{*,c} = 1, 2, 3$ plotted against proto-cluster mass. The values 1 and 0.7 are used for the Larson relation $\rho \propto R^{-\gamma}$. As for the polytropic index $\Gamma$ of gas inside the proto-cluster, values 1 (isothermal) and 0.85 are considered. The Jeans mass is plotted with thin curves, and the IMF peak mass is plotted with thick curves. Color codings are same as those in Fig. 4.

## 3 Conclusions

One important message is that stars do not form uniformly in molecular clouds. In this study, we confronted observations and simulations with a simple analytical model. We showed that before stars start forming, the molecular cloud gas is reprocessed through gravo-turbulent interaction and a gaseous proto-cluster environment

in global equilibrium is established, which is much more favorable for star formation than the diffuse large-scale molecular clumps. This gaseous proto-cluster sets a more general condition for stellar cluster formation and to some extent decouples star formation from the large-scale molecular clump. This is supports the idea that stellar clusters form in similar environments and that the IMF is regulated by more local conditions. We developed a two-dimensional model for a system with rotation, turbulence, and accretion, which predicts the radius, aspect ratio, and velocity dispersion given the mass, angular momentum, and accretion rate of the system. Readers interested by more details are invited to refer to Lee & Hennebelle (2016b).

The gaseous proto-clusters lie on an equilibrium sequence that is governed by the interaction of gravity and turbulence, which yields a mass-size relation similar to the Larson relation, while a gaseous proto-cluster is roughly ten times more massive than a molecular cloud of the same size. Such a resemblance is seen in the two relations since both are outcomes of turbulence and gravity interaction. Notwithstanding, we emphasize that in the case of a gaseous proto-cluster, accretion is relatively important in concentrating mass and sustaining turbulence, thus creating an environment different from that of the molecular cloud. As most stars form in clusters, the gaseous proto-cluster properties should be indeed used for understanding star formation. Using a simple estimate for the peak position of the CMF, we show that because of various compensations, it depends only weakly on the cluster mass, which suggests that the physical conditions of gaseous proto-clusters may be, at least in part, responsible for the apparent universality of the IMF.

This work was granted access to HPC resources of CINES under the allocation x2014047023 made by GENCI (Grand Equipement National de Calcul Intensif). This research has received funding from the European Research Council under the European Community's Seventh Framework Programme (FP7/2007-2013 Grant Agreement no. 306483).

## References

Allen, L., Megeath, S. T., Gutermuth, R., et al. 2007, Protostars and Planets V, 361
Burkert, A. & Bodenheimer, P. 2000, ApJ, 543, 822
Davies, B., Bastian, N., Gieles, M., et al. 2011, MNRAS, 411, 1386
Dib, S., Hennebelle, P., Pineda, J. E., et al. 2010, ApJ, 723, 425
Falgarone, E., Hily-Blant, P., & Levrier, F. 2004, Ap&SS, 292, 89
Falgarone, E., Pety, J., & Hily-Blant, P. 2009, A&A, 507, 355
Fall, S. M., Krumholz, M. R., & Matzner, C. D. 2010, ApJ, 710, L142
Federrath, C., Roman-Duval, J., Klessen, R. S., Schmidt, W., & Mac Low, M.-M. 2010, A&A, 512, A81
Goldbaum, N. J., Krumholz, M. R., Matzner, C. D., & McKee, C. F. 2011, ApJ, 738, 101
Hénault-Brunet, V., Gieles, M., Evans, C. J., et al. 2012, A&A, 545, L1
Hennebelle, P. 2012, A&A, 545, A147
Hennebelle, P. & Chabrier, G. 2013, ApJ, 770, 150
Hennebelle, P. & Falgarone, E. 2012, A&A Rev., 20, 55
Klessen, R. S. & Hennebelle, P. 2010, A&A, 520, A17
Lada, C. J. & Lada, E. A. 2003, ARA&A, 41, 57
Larson, R. B. 1981, MNRAS, 194, 809
Lee, Y.-N. & Hennebelle, P. 2016a, A&A, 591, A30
Lee, Y.-N. & Hennebelle, P. 2016b, A&A, 591, A31
Lombardi, M., Alves, J., & Lada, C. J. 2010, A&A, 519, L7
Mackey, A. D., Da Costa, G. S., Ferguson, A. M. N., & Yong, D. 2013, ApJ, 762, 65
Matzner, C. D. & Jumper, P. H. 2015, ApJ, 815, 68
McKee, C. F. & Ostriker, E. C. 2007, ARA&A, 45, 565
Pfalzner, S. 2011, A&A, 536, A90
Pfalzner, S., Kirk, H., Sills, A., et al. 2016, A&A, 586, A68
Urquhart, J. S., Moore, T. J. T., Csengeri, T., et al. 2014, MNRAS, 443, 1555